




Improved tensile strength and electrical conductivity in Cu–Cr–Zr alloys by controlling the precipitation behavior through severe warm rolling

D. P. Shen^{1,2} , N. Xu¹, M. Y. Gong¹, P. Li¹, H. B. Zhou¹, W. P. Tong^{1,*}, and Gerhard Wilde²

¹Key Laboratory of Electromagnetic Processing of Materials (Ministry of Education), Northeastern University, Shenyang 110819, China

²Institute of Materials Physics, Westfälische Wilhelms-Universität Münster, 48149 Münster, Germany

Received: 30 November 2019

Accepted: 18 May 2020

© Springer Science+Business Media, LLC, part of Springer Nature 2020

ABSTRACT

A Cu–Cr–Zr alloy was subjected to severe warm rolling, and the effects of processing temperature and strain on the precipitation and microstructures were systematically studied. The results show that the nucleation and growth of precipitates interact with the deformation-induced defects, and therefore, the distribution precipitates vary with the different warm rolling processes. This leads to a significant impact on mechanical and electrical properties. In detail, the size of the precipitates is coarser, but the number density is lower as the applied strain (after each annealing treatment) and temperature are higher. And therefore, the UTS is lower, but the electrical conductivity is higher in rolled sheets under higher strain and temperature. Moreover, the present process could improve the comprehensive properties of Cu–Cr–Zr alloys, and an excellent combination of high UTS of 586 MPa and good electrical conductivity of 78.2%IACS was achieved in the sample of RRA ~ 723 K. (The sample was subjected to intermediate annealing treatment at 723 K between each of two rolling passes.)

Introduction

Cu–Cr–Zr alloys are one of the most researched materials for electrical applications due to their excellent electrical and thermal conductivities, outstanding tribological characteristics, and high mechanical strength [1–5]. In the last several decades, severe plastic deformation (SPD) has usually been

implemented before aging to refine the grain size and obtain better performance, and a series of encouraging results have been obtained using this process flow [6–14]. For example, an ultra-fine-grained Cu–1Cr–0.1Zr (wt%) alloy prepared by equal-channel angular pressing (ECAP), followed by aging treatment, demonstrated an excellent combination of a high electrical conductivity and high tensile strength

Address correspondence to E-mail: wptong@mail.neu.edu.cn

[6]. Zhang et al. [13] reported that Cu–Cr–Zr strips obtained a high strength and high electrical conductivity by a novel two-stage cryorolling (rolling at liquid nitrogen temperature) process with an intermediate aging treatment.

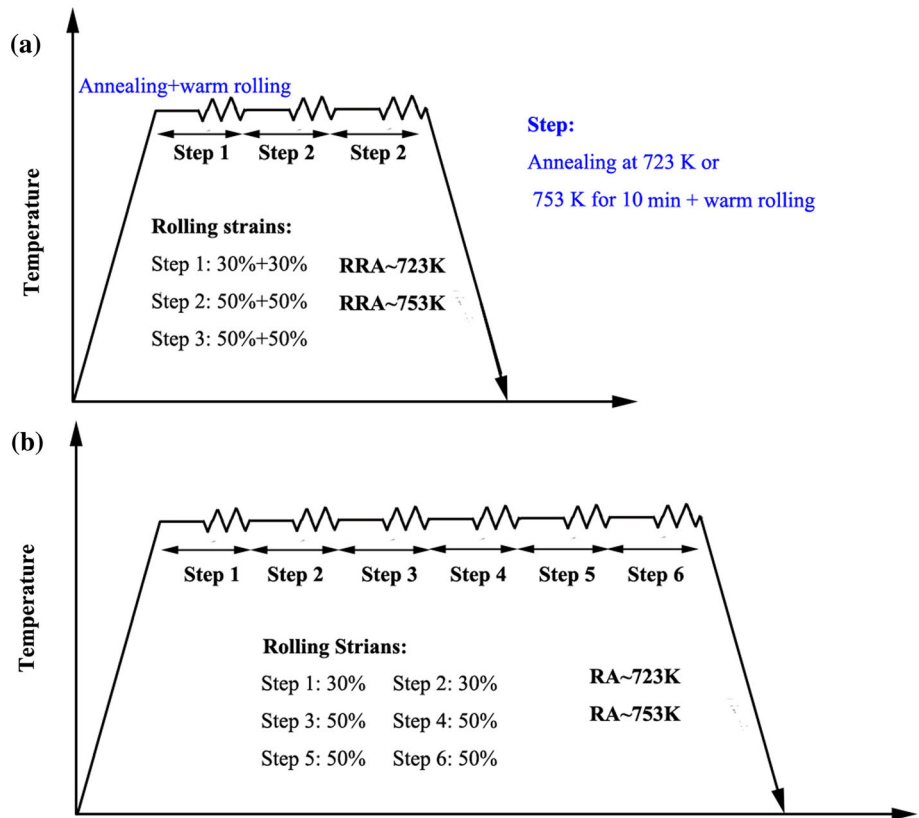
It is generally accepted that besides the development of ultrafine-grained structures and high dislocation densities [15–18], the yield strength (YS) and ultimate tensile strength (UTS) of Cu–Cr–Zr alloys processed by SPD can be enhanced by nanoscale Cr or Heusler phase (CrCu₂Zr) particles through dispersion strengthening [19, 20], which were induced by the precipitation of solute atoms. The size and the number density of the precipitates play an important role in strengthening effect. Additionally, the volume fraction of the precipitates plays a critical role in determining the electrical conductivity of Cu–Cr–Zr alloys [21, 22]. Specifically, the higher the precipitates volume fraction, the lower the solute atoms remained in the matrix, thereby reducing the effect of electron scattering caused by solutes atoms and increasing the electrical conductivity. Therefore, it is very important to control the behavior of the precipitation. However, up to now, one-step aging treatments followed with severe plastic deformation are the main methods for inducing precipitates and therefore to obtain excellent combination properties with high strength and high electrical conductivity in Cu–Cr–Zr alloys [23, 24]. Previous studies [25–27] have shown that deformation straining at elevated temperatures can change the precipitation behavior in steel and Al alloys, which indicated that the shear bands and dislocation substructures produced by intensive straining could change precipitation kinetics during deformation, due to the reason that the shear bands and dislocations can serve as pathways for short-cut diffusion with lower diffusion activation energy [28]. Therefore, the precipitates that originated from deformation strain at elevated temperatures were different from the precipitates formed under static conditions [29]. The above process could be regarded as a method for modifying the precipitation behavior, but few studies have been conducted on strain-induced precipitation in Cu–Cr–Zr alloys at elevated temperatures. Therefore, in the present study, the effect of strain and temperature of warm rolling on the precipitation and microstructure was studied.

Method

A commercial C18150 with 1.0 wt% Cr and 0.1 wt% Zr alloy was chosen in the present work and firstly subjected to solution treatment, which was heated at 1000 °C for 1 h and immediately quenched in cold water. Then, it was cut into specimens by wire-electrode cutting with the size of 40 mm × 40 mm × 80 mm. And the samples were subjected to six-pass warm rolling with a total strain of 97%, and finally, strain of 97% in total of a thin sheet with the thickness of 1.25 mm has been obtained. The roll diameter and roll speed were 105 mm and 30 rpm, respectively. Two of the samples were subjected to annealing at 723 K or 753 K for 10 min before each of two rolling passes, and are labeled as RRA ~ 723 K and RRA ~ 753 K, respectively. The detailed routes are illustrated in Fig. 1a. While for another two samples, the annealing treatment (at 723 K or 753 K for 10 min) is applied before each of rolling passes, and samples are labeled as RRA ~ 723 K and RRA ~ 753 K, as shown in Fig. 1b. And finally, the samples were cooled in air after the final pass.

The samples characterized by scanning electron microscopy (SEM) and electron back-scattered diffraction (EBSD) were prepared by mechanical grinding and polishing, followed by electro-polishing. And the step size of 140 nm was chosen for all EBSD scans. The microscopic structure parameters like distribution of grain size and grain boundary misorientation were analyzed by TSL OIM software. And the distribution of grain size was measured using the linear intercept method. The microstructure of the Cu–Cr–Zr alloy was also characterized using a Jeol-4000FX transmission electron microscope (TEM) with an operating voltage of 200 kV. Thin foils for TEM were prepared by mechanical polishing and twin jet polished using a solution of HNO₃ and methanol (1:3) at –20 °C and 15 V. Electrical testing was performed by an intelligent eddy current low-resistance tester. The tensile test samples were designed to be flat with a gauge length of 5 mm, and tensile tests were performed on an IDW-200H universal testing machine with an initial strain rate of 5×10^{-3} mm/s. Three samples were tested for each material condition to ensure the reproducibility of strength and elongation measurements.

Figure 1 Schematic illustration of the severe warm rolling experiments.



Results

Mechanical properties and electrical conductivity

Figure 2 shows the tensile curves of the Cu–Cr–Zr alloy after different severe warm rolling treatments. The tensile strengths and uniform elongations of the prepared samples varied depending on which warm rolling processes (RRA or RA) and annealing temperature (723 K or 753 K) were applied. In detail, under the same annealing temperature, compared with the process of RRA, the ultimate tensile strength (UTS) is higher in the samples applied by RA. For example, the UTS of RRA ~ 723 K is about 586 MPa, which is lower than RA ~ 723 K (approximately 645 MPa), while under the same rolling process, the lower the annealing temperature (723 K), the higher the UTS. However, the elongation at fracture has no clear correlations with temperature or strain rate. In detail, under the annealing temperature of 723 K, compared with the process of RRA, the elongation at fracture is lower in the samples applied by RA. However, under the higher temperature of 753 K, the elongation at break of samples obtained by RRA is

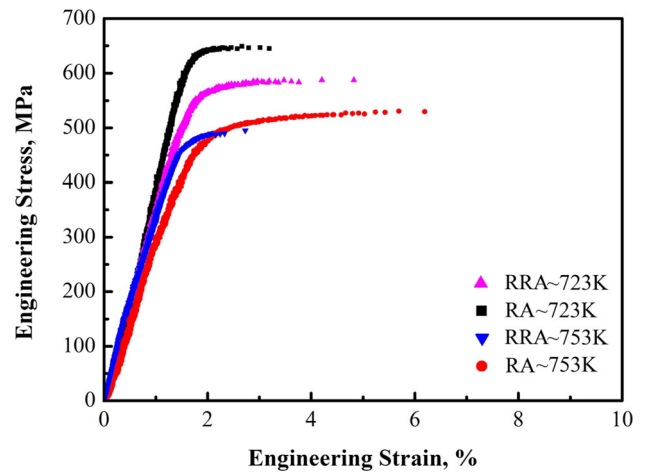


Figure 2 The engineering stress–strain curves of Cu–Cr–Zr alloys subjected to severe warm rolling.

much lower than RA. The reasons for the above phenomena may be related to the dislocation density, grain size as well as the size and distribution of precipitates. Relevant studies have shown that the elongation of deformed metals decreases with the decrease in grain size [6]. Under 723 K, the grain size obtained by RRA is smaller than RA. Thus, its elongation at break should be lower, but the result is

exactly the opposite, as shown in Fig. 2. Therefore, it is plausible to suppose that the size and distribution of the precipitates affect the elongation. Under 723 K, due to lower density of the precipitates in the sample applied by RRA, more dislocations can slide freely in the copper matrix, resulting in higher elongation, while under the higher 753 K, the elongation of the sample obtained by RRA is very poor and much lower than that the sample applied by RA. This is caused by mainly two factors. On the one hand, the grain size of the sample processed by RRA is smaller. On the other hand, the size of precipitates in the sample of RRA is much larger and its distribution is not uniform, which will cause stress concentration near the precipitates. This means that microcracks tend to form near the precipitates and thus have a negative impact on its elongation.

Figure 3 shows the electrical conductivities of RRA ~ 723 K, RA ~ 723 K, RRA ~ 753 K, and RA ~ 753 K, compared with the as-soluted (ST) coarse-grained materials subjected to annealing at 723 K and 725 K for 15 min, 30 min and 60 min, respectively. The ST showed a rapid increase in its electrical conductivity at the early aging stage due to the decomposition of the supersaturated solid solution. Then, the conductivity increased more slowly with longer annealing times as the solute concentration in the matrix approached equilibrium. According to the processes given in Fig. 1, the annealing times for RRA ~ 723 K, RRA ~ 723 K, RRA ~ 753

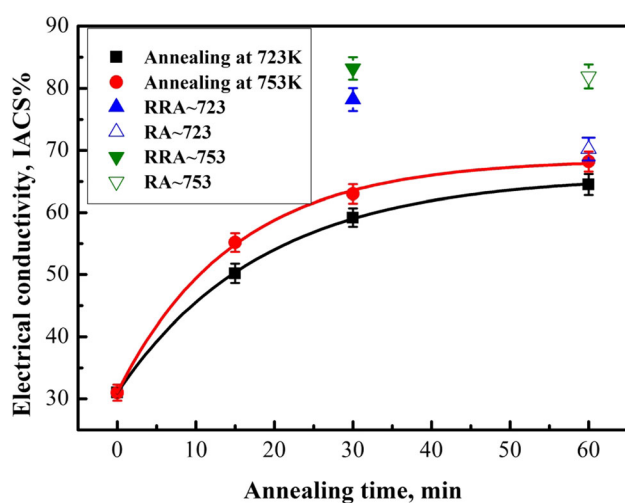


Figure 3 The electrical conductivity of as-soluted Cu–Cr–Zr alloys subjected to severe warm rolling compared with the samples annealed at 723 K and 753 K for 15 min, 30 min, and 60 min, respectively.

K, and RA ~ 753 K were 30 min, 60 min, 30 min, and 60 min, respectively. It is interesting to observe that the electrical conductivity of the solution-treated Cu–Cr–Zr alloy subjected to severe warm rolling is higher than the ST annealed for the same time and at the same temperature. For example, the electrical conductivity of RRA ~ 753 K was 83.2%IACS, which was much higher than the electrical conductivity of the ST alloy annealed at 753 K for 30 min (63.0%IACS). In addition, the results indicate that the electrical conductivity varies with the different warm rolling processes. Specifically, under the same annealing temperature, compared with the process of RA, the electrical conductivity is higher in the samples applied by RRA. For example, the electrical conductivity of RRA ~ 723 K was 78.2%IACS, which is much higher than RA ~ 723 K (approximately 70.2%IACS), while under the same rolling process, the lower the annealing temperature (723 K), the lower the electrical conductivity.

Microstructure

The results indicate that the microstructure of the initial as-soluted Cu–Cr–Zr alloy consists mainly of the equiaxed coarse grains, as shown in Fig. 4a. In addition, there are few Cr-rich particles in the matrix, which means most of Cr has been dissolved into Cu matrix, as shown in Fig. 4b. The microstructures evolved into lamella structures after severe warm rolling, as shown in Figs. 5a–d and 6a–d. The elongation of original grains along the rolling direction is separated from each other by mainly HAGBs. And in the interior of elongation grains, there are some LAGBs and the elongation grains are further divided into subgrains, as shown in Fig. 6a–d. The structural information such as grain size and misorientation distributions was obtained by analyzing the data of EBSD, as shown in Fig. 6e–m. The results indicate that the grain size and misorientation distribution vary with rolling processes (RRA or RA) and annealing temperature (723 K or 753 K). Specifically, under the same annealing temperature, compared by the process of RA, the grain size is smaller, but the fraction of HAGBs is higher in the samples applied by RRA. For example, the average grain size and the fraction of RRA ~ 723 K are 1.69 μm and 55.2%, respectively, while the mean grain size of RA ~ 723 K increased to 1.98 μm , and the fraction of HAGBs reduced to 52.8%. This phenomenon is more obvious

Figure 4 **a** Typical EBSD orientation maps and **b** SEM micrographs of as-soluted alloys.

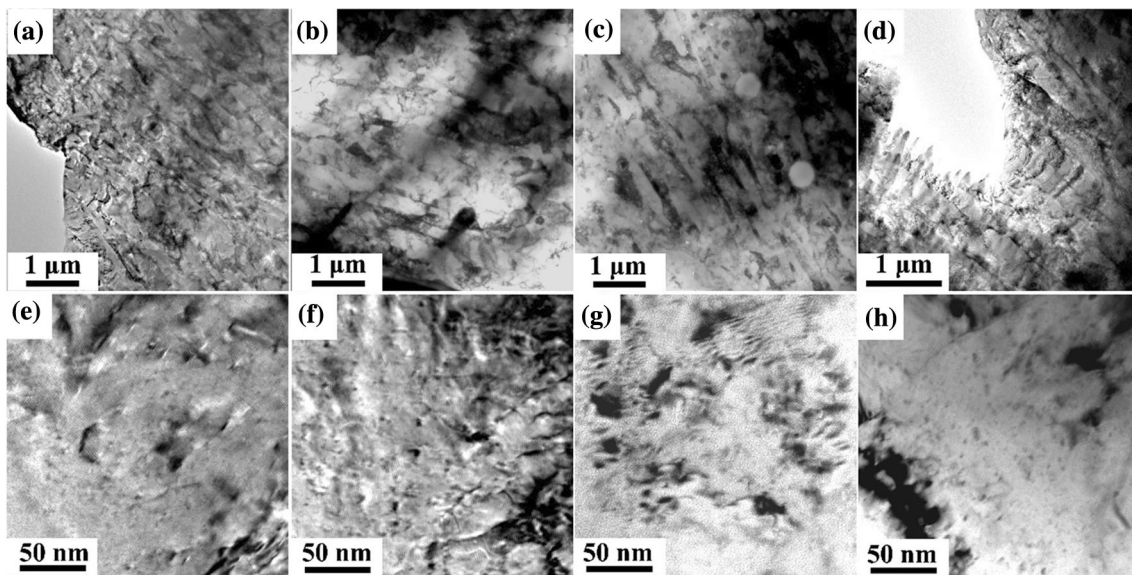
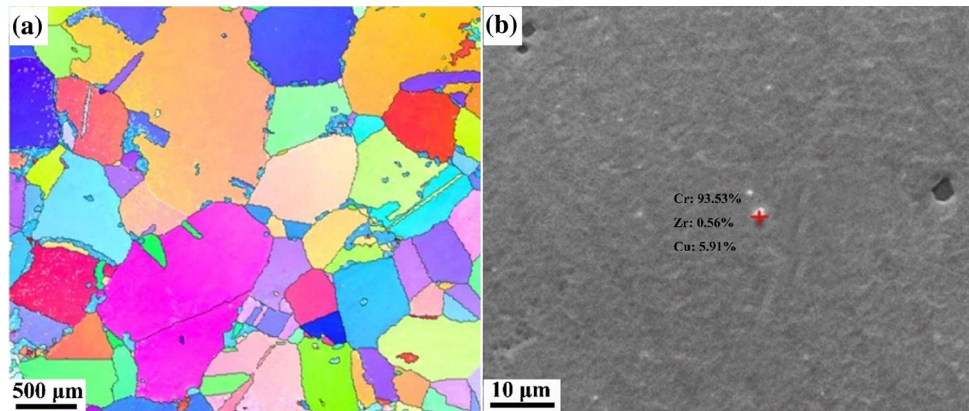
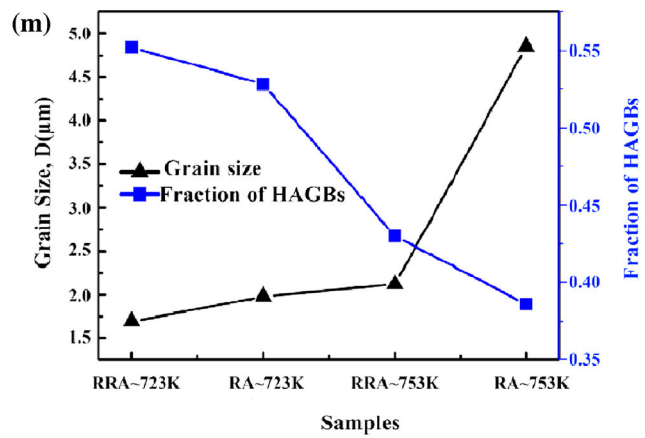
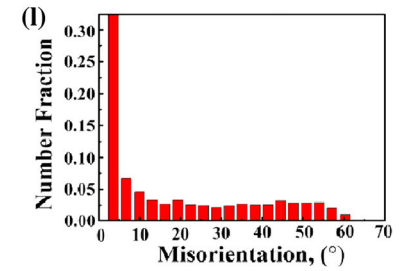
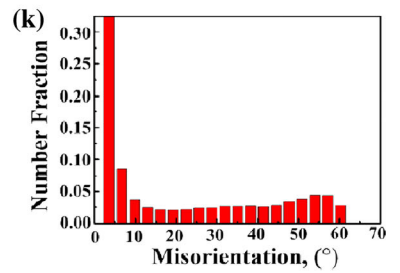
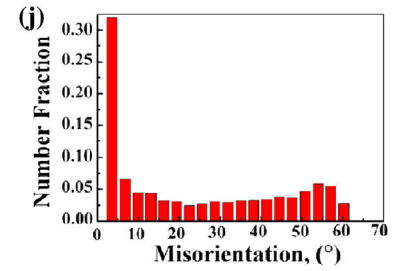
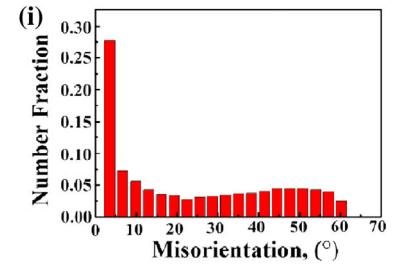
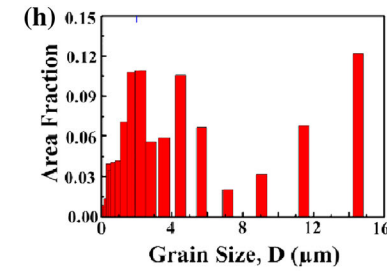
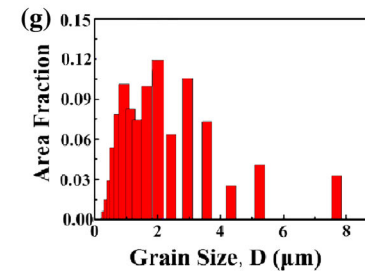
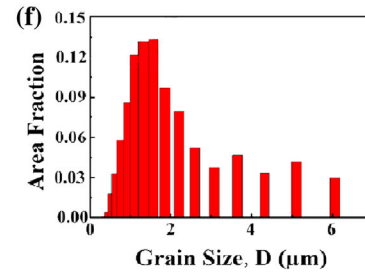
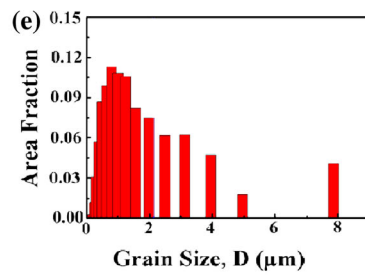
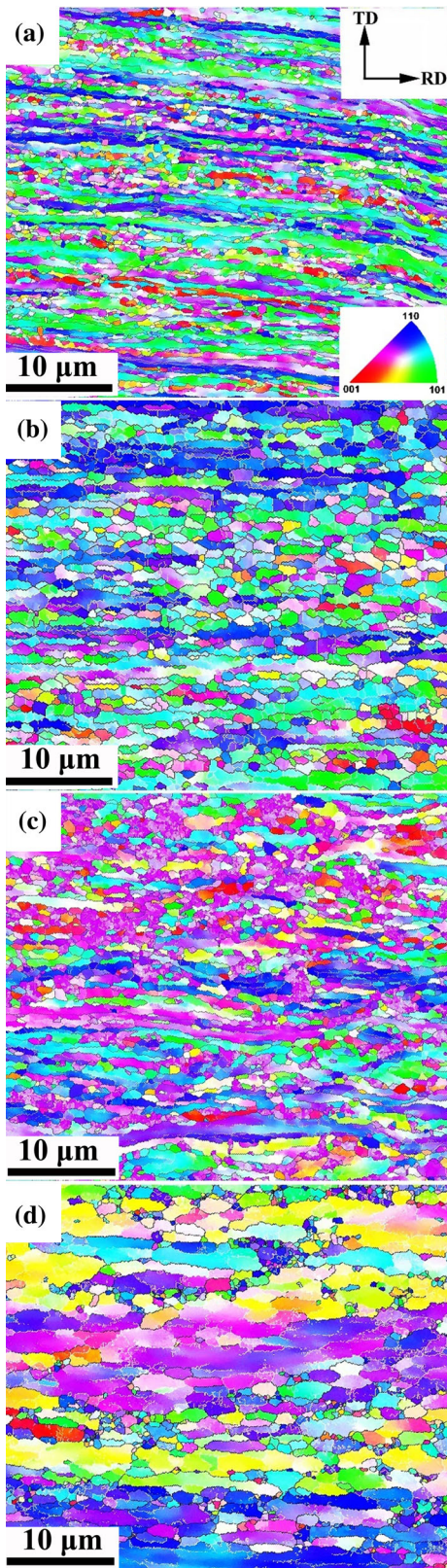


Figure 5 **a–d** The cross-sectional TEM images and **e–h** the TEM micrographs illustrating the precipitates.

at higher annealing temperatures. For example, the average grain size and the fraction of HAGBs of RRA \sim 753 K are 2.12 μm and 43.0%, respectively, while the grain size of RA \sim 753 K increased to 4.85 μm and the fraction of the HAGBs reduced to 38.6%. However, under the same rolling process, the lower the annealing temperature (723 K), the smaller but the higher the fraction of HAGBs.

The previous study reveals that the microstructural evolution in the Cu–Cr–Zr alloy induced by deformation at elevated temperature and those of pure copper subjected to intense plastic straining at ambient temperature [30, 31] are nearly the same. With the increase in strain, the grain refinement process includes: (1) the formation of dislocation cells; (2) the evolution of dislocation walls into LAGBs and thereby dividing the original grains into

several single subgrains; (3) the transformation of LAGBs into HAGBs. Therefore, the warm rolling strain increases the evolution of dislocation walls into LAGBs and further evolves into HAGBs. Under the same annealing temperature, although the total strain of RRA and RA is the same, the continuous two rolling passes are carried out after annealing treatment and therefore the applied strain after annealing is higher than that RA. In addition, the total annealing time of RRA is 30 min, which is much lower than RA (60 min), so it is more likely to form and retain the deformation-induced HAGBs. Under the same rolling process, the lower the temperature, the lower the dynamic recovery, and this is beneficial to the accumulation of dislocations and the evolution of the HAGBs.



◀ **Figure 6 a–d** Typical deformation microstructures of RRA ~ 723 K, RA ~ 723 K, RRA ~ 753 K, and RA ~ 753 K samples, respectively. The white and black lines indicate the low-angle ($\theta < 15^\circ$) and high-angle ($\theta \geq 15^\circ$) boundaries, respectively. The inverse pole figures are shown for the rolling direction (RD) and normal direction (ND) of the rolled samples. **e–h** Corresponding grain size distributions; **i–l** the misorientation distributions; **m** as well as the mean size and the fraction of HAGBs.

The morphology and distribution of Precipitates

Figure 7a–d shows the distribution of precipitated chromium particles in RRA ~ 723 K, RA ~ 723 K, RRA ~ 753 K, and RA ~ 753 K samples, respectively. The morphologies of chromium particles in the above samples are shown in Fig. 7e–h. Based on the SEM images in Fig. 7a–d, the sizes of Cr particles coarser than 200 nm were measured three times by the software of Image J, and the corresponding size distribution is shown in Fig. 8a. In addition, the statistical results such as the mean sizes and densities of

particles are shown in the inset image in Fig. 8a. The results indicate that the morphology, size, and the number density of the precipitated Cr particles vary with the different warm rolling processes. Specifically, under the same annealing temperature, the mean size of particles is larger, but the number density is lower in the samples applied by RRA than RA. For example, the average size and the number density of particles in RRA ~ 723 K are $0.62 \pm 0.06 \mu\text{m}$ and $(1.82 \pm 0.04) \times 10^4/\text{m}^2$, while the corresponding data in RA ~ 723 K are $0.54 \pm 0.04 \mu\text{m}$ and $(2.78 \pm 0.08) \times 10^4/\text{m}^2$, respectively. This phenomenon is particularly evident at 753 K. The average particle size of RRA ~ 753 K is approximately $1.0 \pm 0.12 \mu\text{m}$, and some abnormal coarser particles larger than $5 \mu\text{m}$ are observed (Fig. 7c), which is much larger than RA ~ 753 K ($0.59 \pm 0.04 \mu\text{m}$). And the number density of particles is also as low as $(1.05 \pm 0.04) \times 10^4/\text{m}^2$, which is much lower than RA ~ 753 K ($(3.57 \pm 0.11) \times 10^4/\text{m}^2$). Under the same process (RRA or RA), compared with the samples annealed at 723 K, the mean size of precipitates is larger, but the

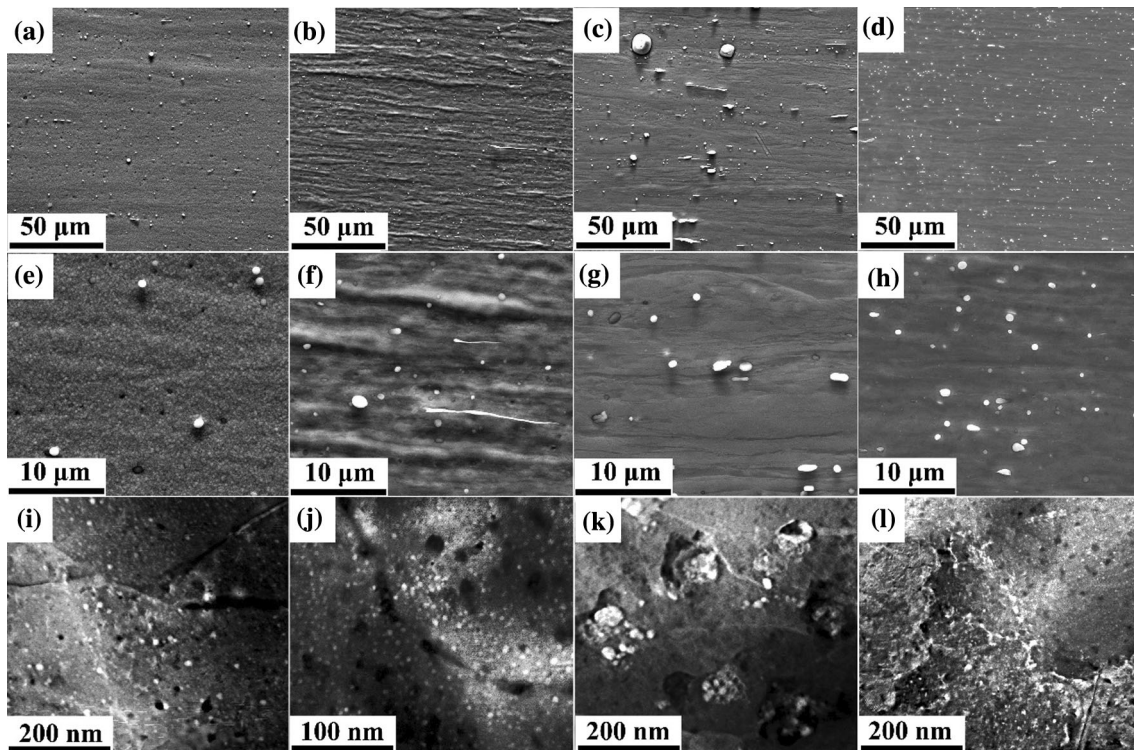
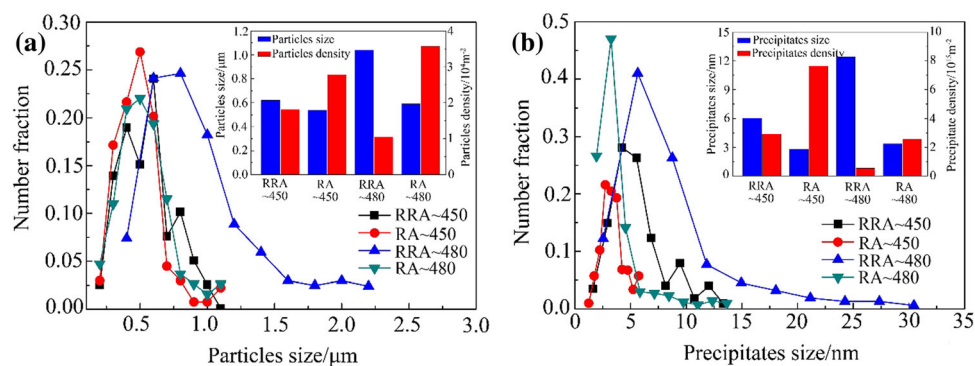


Figure 7 a–d SEM micrographs showing the distribution of Cr particles in the samples of RRA ~ 723 K, RA ~ 723 K, RRA ~ 753 K, and RA ~ 753 K, respectively; **e–**

h corresponding morphologies of the above samples; and **i–l** corresponding precipitate distribution characterized by STEM.

Figure 8 **a** Size distribution, mean size, and number density (as shown in the inset image) of particles larger than 200 nm; **b** and for precipitates smaller than 100 nm in RRA ~ 723 K, RA ~ 723 K, RRA ~ 753 K, and RA ~ 753 K, respectively.



number density is lower in the samples annealed at 753 K. In addition, the morphology of chromium particles is also affected by different processes and annealing temperatures. For example, most of Cr particles in RRA ~ 723 K, RA ~ 723 K, and RA ~ 753 K are mostly spherical, while most of the particles in RRA ~ 753 K were irregular, as shown in Fig. 7g.

Aside from the precipitated chromium particles, there are nanoscaled precipitates with various number density according to the samples, as shown in Fig. 5e–h. The precipitates exhibit various contrasts and are easily entangled with dislocations in bright-field TEM images, making it difficult to get their statistical information. Therefore, the STEM images were further collected, as shown in Fig. 7i–l. The size distribution and number density of precipitates were measured through STEM images. And the sizes and number of precipitates smaller than 50 nm were counted with two times by the software of Image J, and the corresponding grain size distribution is shown in Fig. 8b. In addition, the statistical analysis of the mean sizes and densities of precipitates is shown in the inset image. The results indicate that the size and the number density of the precipitates also vary with the different warm rolling processes and annealing temperature, and the trend is similar to Cr particles. In detail, under the same annealing temperature, the mean size of particles is larger, but the number density is lower in the samples applied by RRA than RA. For example, the average size and the number density of precipitates in RRA ~ 723 K are 6.0 ± 0.4 nm and $(2.9 \pm 0.11) \times 10^{15}/\text{m}^2$, while the corresponding data in RA ~ 723 K are 2.78 nm and $7.64 \times 10^{15}/\text{m}^2$, respectively. This phenomenon is particularly evident at 753 K. The average size of precipitates in RRA ~ 753 K is approximately 12.4 nm, and some abnormal coarser particles larger

than 20 nm were observed (Fig. 5k), which is much larger than RA ~ 753 K (3.4 ± 0.2 nm). And the number density of particles is also as low as $(0.54 \pm 0.05) \times 10^{15}/\text{m}^2$, which is much lower than RA ~ 753 K ($(2.56 \pm 0.12) \times 10^{15}/\text{m}^2$). Under the same process (RRA or RA), compared with the samples annealed at 723 K, the mean size of precipitates is larger, but the number density is lower in the samples annealed at 753 K. For example, the average precipitates size and the number density of RRA ~ 723 K are 6.0 ± 0.4 nm and $(2.9 \pm 0.11) \times 10^{15}/\text{m}^2$, while the corresponding data in RRA ~ 753 K are 12.4 nm and $0.54 \times 10^{15}/\text{m}^2$, respectively. As discussed above, the size distribution and number density of precipitates could be affected by the rolling temperature and processes. It should be noticed that the RRA-753 samples are significantly coarsened and their density decreases significantly, as shown in the figure. It should be noted that a number of precipitates adhere to each other or have been grown in the sample of RRA-753, as shown in Fig. 7k. This suggests that the new precipitates may nucleate and grow near the original precipitates.

Discussion

The effect of severe warm rolling on precipitation

Experiments showed that the distribution of chromium particles and precipitates vary with the different warm rolling processes. Essentially, this is caused by the interaction between the nucleation and growth of precipitates with the warm deformation-induced defects. As is well known, the nucleation barrier (ΔG^*) for classical nucleation of precipitates can be expressed as follows:

$$\Delta G^* = \frac{16\pi}{3} \frac{\gamma^3}{(\Delta g_n + \Delta g_e)^2} \quad (1)$$

where Δg_n , Δg_e , and γ are the driving force, elastic energy of the precipitates, and the interfacial energy, respectively. The dislocations and vacancy clusters induced by warm rolling can decrease the interfacial and elastic energies of the precipitates [26]. In addition, the “Cottrell atmosphere” effect caused by dislocations can induce the segregation of solute atoms and increase the concentration of solute atoms near dislocations. The dislocations could then act as diffusion tubes with lower diffusion activation energies, and the nucleation could be accelerated by the pipe diffusion of solute atoms through dislocations [28]. Therefore, the nucleation of precipitates is more likely to occur at sites containing a large amount of crystal defects, such as dislocations and vacancy clusters. Based on the above discussion, we proposed an explanation why the size and number density of the Cr particles and precipitates vary with the different warm rolling processes. Under the same annealing temperature, although the total strain of RRA and RA is the same, the continuous two rolling passes are carried out after annealing treatment in RRA and therefore, the applied strain after annealing is higher than that RA. Therefore, after each annealing treatment, the RRA exerts a higher strain level than the RA, which continuously produces higher density defects such as dislocations, dislocation walls, and vacancy clusters, thereby the speed of nucleation and growth of precipitates is higher, which means that the precipitated Cr particles and precipitates are more likely to be coarsened. The coarsening of the precipitated phase could accompany by the combination of precipitates and form the solute atoms depleted region, and therefore, the number density is relatively lower. Hence, under the same annealing temperature, compared with RA, the mean size of particles and precipitates is larger, but the number density is lower in the samples applied by RRA. Similarly, under the same process (RRA or RA), compared with the samples warm rolling after annealed at 723 K, the diffusion coefficient of sample warm rolling after annealed at 753 K is higher, thereby the growth speed of precipitates is higher. Thus, as talked above, the size of the particles and precipitates is larger, but the number density is lower.

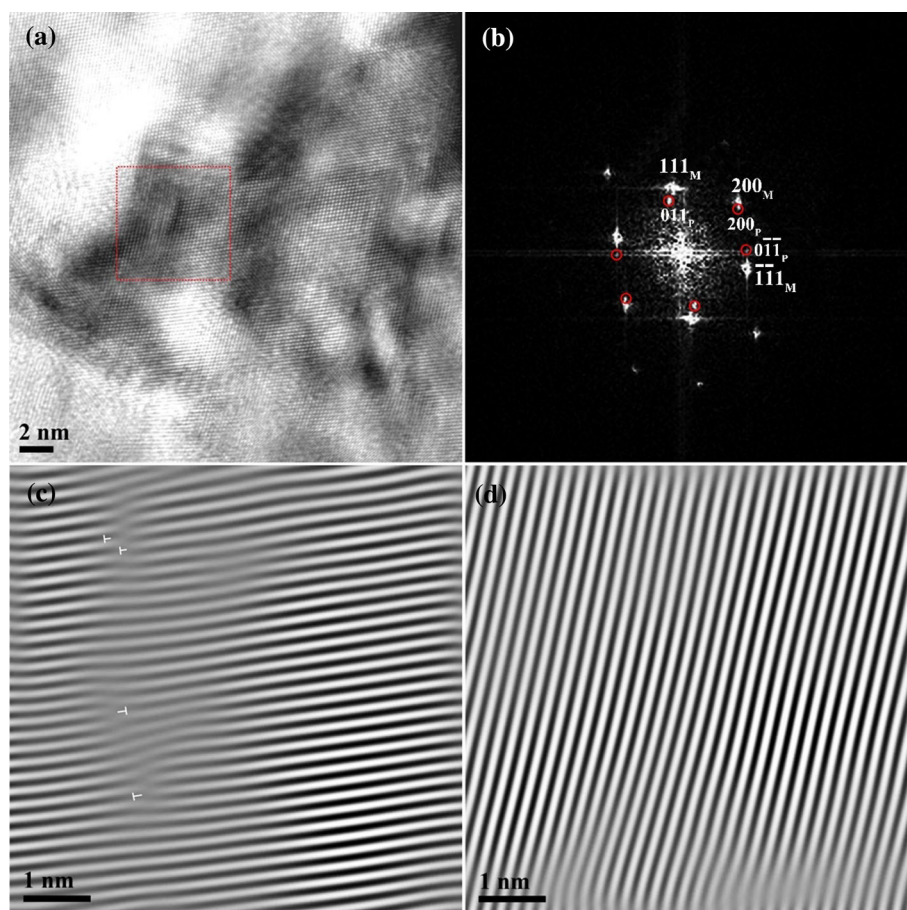
As talked above, the nucleation and growth of precipitates interact with the deformation-induced defects. However, the evolution of precipitates during the process of warm rolling is not clear. In the present study, the precipitate is further analyzed by high-resolution transmission electron microscope (HRTEM) and tries to explain the evolution rule of precipitates according to the observed phenomenon.

A high-resolution TEM (HRTEM) image shows two kinds of typical Cr-rich precipitates, as shown in Figs. 9 and 10. The first one shows a rod-shaped morphology when observed under [011] zone axis conditions. By indexing the diffraction patterns in Fig. 9b, the precipitate was verified to show Kurdjumov–Sachs orientation relationships with copper matrix [32]. The second kind of precipitate exhibits pea-shaped contrast, which is a typical coherent precipitate [32, 33]. And there are no diffraction spots other than copper in the diffraction spots, as shown in Fig. 10b, which is also a typical feature of the coherent precipitate [32, 33]. In addition, a certain density of dislocations was observed around the precipitates (Figs. 9 and 10), which were caused by a misfit between the precipitates and Cu matrix.

The results further verify that the dislocations were introduced by warm rolling interactions with the precipitates. The evolution rule of precipitates interacts with the warm rolling-induced defects can be interpreted with the following model, as shown in Fig. 11:

1. The dislocations introduced by warm rolling act as diffusion tube and draw solute atoms to these sites which induce the segregation of Cr atoms near dislocations. The diffusion coefficient of Cu in bcc Cr at 713 K ($4.1 \times 10^{-17} \text{ cm}^2 \text{ s}^{-1}$ [34]) is two orders of magnitude smaller than that of Cr in fcc Cu ($1.5 \times 10^{-15} \text{ cm}^2 \text{ s}^{-1}$ [35]). The rolling temperatures in the present work were, respectively, 723 K and 753 K, which are near 713 K. Thus, compared with the migration rate of Cu atoms, the ejections of Cr atoms from the Cu matrix will require less time to migrate to dislocations, and the segregation of Cr atoms occurs more easily.
2. Regions with enriched solute atoms are formed near dislocations due to the segregation of Cr atoms, which promotes the nucleation and growth of embryos and stable precipitates. Due to the misfit between embryos and precipitates and the Cu matrix (Fig. 9 and 10), the embryos

Figure 9 **a** HRTEM image of the first type of precipitate embedded in the Cu matrix, **b** fast Fourier transform (FFT) corresponding to (a), inverse fast Fourier transform (IFFT) images, **c** using only $(\bar{1}\bar{1}1)$ and **d** using only $(1\bar{1}1)$ reflection.



and precipitates acted as an effective barrier for dislocation glide and therefore accumulate high density dislocations. These dislocations further induced the segregation of solute atoms toward these dislocation structures.

3. Many newly nucleated precipitates appeared near the original precipitates because of the interaction between dislocations and precipitates.
4. Due to the formation of many precipitates, the precipitates coalesced and formed coarser precipitates. It should be noted that due to the large number of precipitates formed near dislocations, it is inevitable to form Cr poor area, which would result in a sharp decline in the number density of precipitates in Cr poor area. The RRA \sim 753 K sample is the most typical case, as shown in Fig. 7k.

The effect of severe warm rolling on electrical conductivity and mechanical properties

The present experiments showed that the electrical conductivity and mechanical properties vary with different warm rolling processes. Essentially, this is caused by different microstructures and the precipitation features after different deformation conditions.

Although higher density of grain boundaries and dislocations were induced by severe warm rolling, the electrical conductivities of RRA \sim 723 K, RA \sim 723 K, RRA \sim 753 K, and RA \sim 753 K alloys are higher than the ST subjected to annealing for the same time at an identical temperature. Considering the fact that there is a strong negative correlation between the content of solute atoms and the electrical resistivity [4], the higher electrical conductivity of the warm-rolled samples is caused by the lower solute atoms content. That is to say, severe warm rolling could accelerate the progress of solid solution decomposition and precipitation. In addition, the

Figure 10 **a** HRTEM image of the second type of precipitate embedded in the Cu matrix, **b** fast Fourier transform (FFT) corresponding to (a), inverse fast Fourier transform (IFFT) images, **c** using only $(\bar{1}\bar{1}1)$ and **d** using only $(1\bar{1}1)$ reflection.

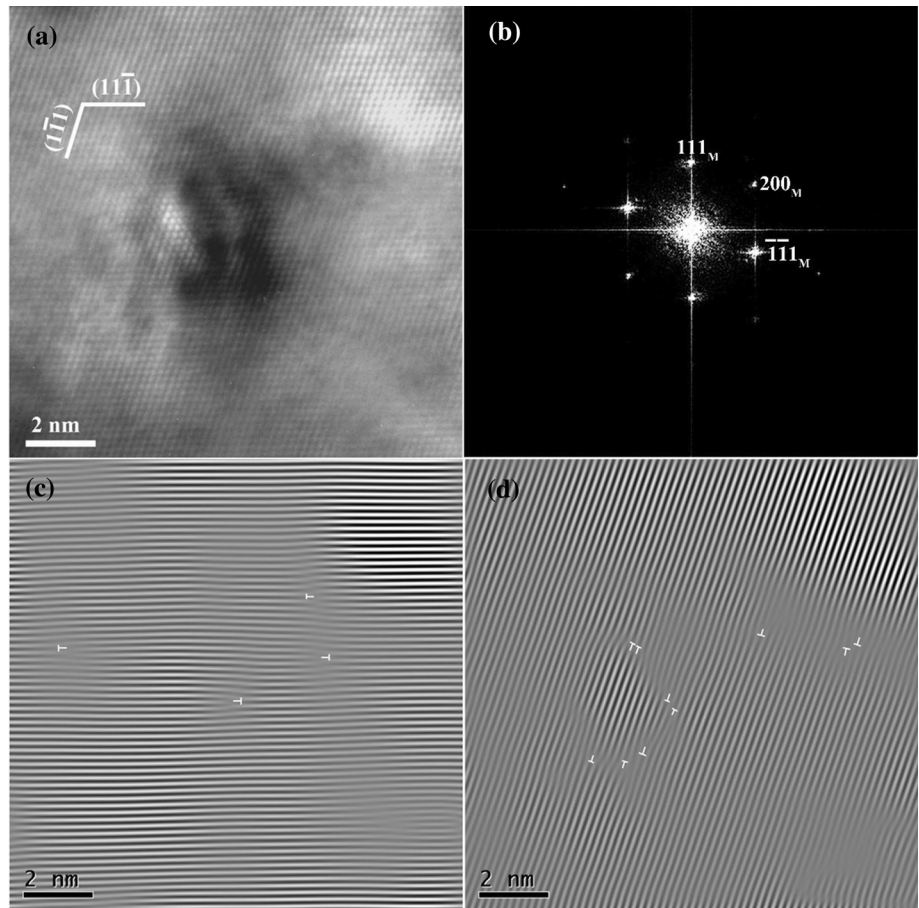
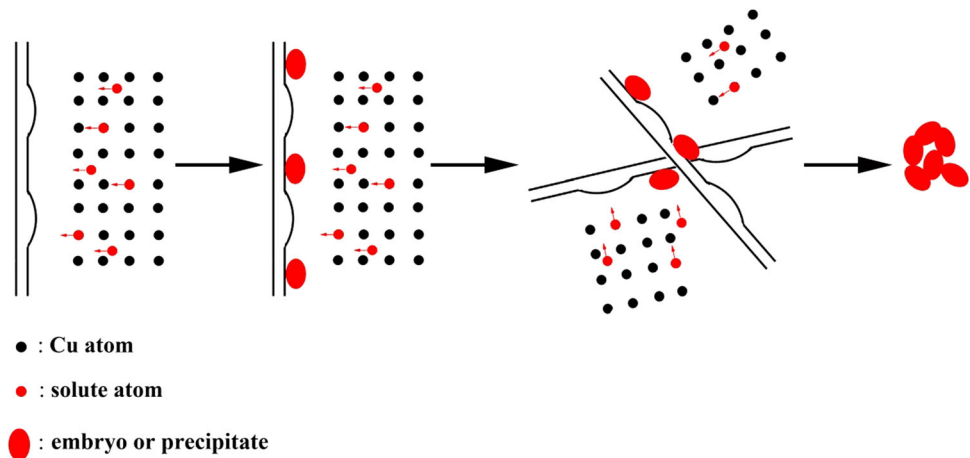


Figure 11 Schematic illustration of the dislocation interaction with the precipitate.



above results also indicate that under the same annealing temperature, compared with the process of RA, the electrical conductivity is higher in the samples applied by RRA even though the total annealing time is much shorter. Similarly, under the same process (RRA or RA), compared annealed at 723 K, the electrical conductivity is higher in the samples

annealed at 753 K. Therefore, it can be inferred again that the speed of precipitation is higher at higher strain and higher temperatures. This is consistent with the phenomenon observed above, i.e., the Cr particles and precipitates are coarser in the sample applied by RRA and annealed at higher temperature.

The evolution of UTS is similar to electrical conductivities. That is, compared with the process of RRA, the UTS is higher in the samples applied by RA under the same annealing temperature even though the average grain size is smaller. This phenomenon is partly caused the different features of precipitates. Previous study claimed the increase in the yield strength caused by precipitation strengthening can be expressed by Orowan bowing [36]:

$$\sigma_p = 0.84 \text{ MGb}/\lambda \quad (2)$$

where λ is the inter-particle spacing. In the present study, the results show that compared with the samples applied by RA, the precipitates are coarser, but the number density is lower in the sample applied by RRA under the same annealing temperature. Therefore, the value of λ is higher and therefore the effect of precipitation strengthening is lower in the sample applied after RRA. In addition, under the same process (RRA or RA), compared with the samples annealed at 753 K, the UTS is higher annealed at 753 K. The result is expected due to the reason that compared with the samples annealed at 753 K, the grain size and precipitates are finer in the samples annealed at 723 K.

The effect of severe hot rolling on electrical conductivity

As talked above, under the same annealing conditions, compared with the as-soluted sample, the electrical conductivity of the RRA \sim 723, RA \sim 723, RRA \sim 753, and RA \sim 753 is higher. As is well known, the electrical resistivity of Cu–Cr–Zr alloy can be expressed based on the Matthiessen's rule:

$$\rho = \rho_0 + \Delta\rho_S + \Delta\rho_D + \Delta\rho_B \quad (3)$$

where ρ_0 is the electrical resistivity of the ideally pure Cu, $\Delta\rho_S$, $\Delta\rho_D$, and $\Delta\rho_B$ are the residual resistivity caused by solute atoms, dislocation, and grain boundary, respectively. Related studies have also shown that the content of residual solute atoms is closely related to the electrical resistivity [4]. And generally, compared with defect structure like vacancies, dislocations, and grain boundaries, it has a much greater influence on it [4]. As we known, compared with annealed ST sample, the higher density of grain boundaries and dislocations were inevitable induced by above severe warm rolling processes. That means the electrical conductivity of

the samples applied by severe warm rolling would be lower than annealed ST sample due to electron scattering caused by defect structures under the condition that the electrical resistivity caused by solute atoms is the same, but the results are counter to what would be expected. Therefore, it is reasonable to infer that the enhanced electrical conductivity in the severe warm rolling samples is caused by lower content of solute atoms. That is to say, the process of severe warm rolling can accelerate the speed of decomposition from supersaturated matrix. In addition, the results also indicate that under the same annealing temperature, compared with the process of RA, the electrical conductivity is higher in the samples applied by RRA. Similarly, this means the residual solute atoms in the sample applied by RRA is lower than RA. In other words, compared with the process of RA, the process of RRA can further accelerate the speed of precipitation.

Conclusion

The developed microstructures, the evolution of precipitates, and mechanical properties of Cu–1%Cr–0.1%Zr alloy subjected to multiple warm rolling at 723 K and 753 K were investigated. The main results are summarized as follows:

The distribution of chromium particles and precipitates varies with the different warm rolling processes. In detail, under the same annealing temperature, compared with RA, the mean size of particles and precipitates is larger, but the number density is lower in the samples applied by RRA. Similarly, under the same process (RRA or RA), compared with the samples warm rolling after annealed at 723 K, the particles and precipitates are coarser, but the number density is lower in the sample annealed at 753 K. To be more precise, the size of the precipitates is finer, but the number density is higher as the applied strain (after each annealing treatment) and temperature decreased. Moreover, the size distribution and number density of the precipitates are further influencing the mechanical and electrical properties. And the UTS is lower, but the electrical conductivity is higher in rolled sheets under lower strain and temperature.

Acknowledgements

This research was supported by the National Natural Science Foundation of China (U1810109) and China Scholarship Council.

Compliance with ethical standards

Conflicts of interest We declared that we have no conflicts of interest to this work. We declare that we do not have any commercial or associative interest that represents a conflict of interest in connection with the work submitted.

References

- [1] Zhang DL, Mihara K, Tsubokawa S, Suzuk HG (2000) Precipitation characteristics of Cu–15Cr–0.15Zr in situ composite. *Mater Sci Technol* 16:357–363
- [2] Zhilyaev AP, Morozova A, Cabrera JM (2017) Wear resistance and electroconductivity in a Cu–0.3Cr–0.5Zr alloy processed by ECAP. *J Mater Sci* 52:305–313. <https://doi.org/10.1007/s10853-016-0331-8>
- [3] Xu S, Fu H, Wang Y (2018) Effect of Ag addition on the microstructure and mechanical properties of Cu–Cr alloy. *Mater Sci Eng A* 726:208–214
- [4] Shen DP, Zhu YJ, Yang X, Tong WP (2018) Investigation on the microstructure and properties of Cu–Cr alloy prepared by in-situ synthesis method. *Vacuum* 149:207–213
- [5] Zhou HT, Zhong JW, Zhou X, Zhao ZK (2008) Microstructure and properties of Cu–1.0 Cr–0.2 Zr–0.03 Fe alloy. *Mater Sci Eng A* 498:225–230
- [6] Vinogradov A, Patlan V, Suzuki Y, Kitagawa K, Kopylov V (2002) Structure and properties of ultra-fine grain Cu–Cr–Zr alloy produced by equal-channel angular pressing. *Acta Mater* 50:1639–1651
- [7] Huang AH, Wang YF, Wang MS (2019) Optimizing the strength, ductility and electrical conductivity of a Cu–Cr–Zr alloy by rotary swannealing and annealing treatment. *Mater Sci Eng A* 746:211–216
- [8] Shen DP, Zhou HB, Tong WP (2019) Grain refinement and enhanced precipitation of Cu–Cr–Zr induced by hot rolling with intermediate annealing treatment. *J Mater Res Technol* 8:5041–5045
- [9] Ding R, Guo C, Guo S (2013) Assessment of anisotropic tensile strength using a modified shear punch test for Cu–Cr–Zr alloy processed by severe plastic deformation. *Mater Sci Eng A* 587:320–327
- [10] Islamgaliev RK, Nesterov KM, Bourgon J, Champion Y, Valiev RZ (2014) Nanostructured Cu–Cr alloy with high strength and electrical conductivity. *J Appl Phys* 115:194301
- [11] Islamgaliev RK, Nesterov KM, Champion Y, Valiev RZ (2014) Enhanced strength and electrical conductivity in ultrafine-grained Cu–Cr alloy processed by severe plastic deformation. *IOP Conf Series Mater Sci Eng* 63:012118
- [12] Fu HD, Xu S, Li W, Xie JX, Zhao HB, Pan ZJ (2017) Effect of rolling and aging processes on microstructure and properties of Cu–Cr–Zr alloy. *Mater Sci Eng A* 700:107–115
- [13] Zhang SJ, Li RG, Kang HJ et al (2017) A high strength and high electrical conductivity Cu–Cr–Zr alloy fabricated by cryorolling and intermediate aging treatment. *Mater Sci Eng A* 680:108–114
- [14] Sun L, Tao NR, Lu K (2015) A high strength and high electrical conductivity bulk CuCrZr alloy with nanotwins. *Scripta Mater* 99:73–76
- [15] Sakai T, Belyakov A, Kaibyshev R, Miura H, Jonas JJ (2014) Dynamic and post-dynamic recrystallization under hot, cold and severe plastic deformation conditions. *Prog Mater Sci* 60:130–207
- [16] Estrin Y, Kim HS, Nabarro FR (2007) A comment on the role of Frank-Read sources in plasticity of nanomaterials. *Acta Mater* 55:6401–6407
- [17] Bouaziz O, Estrin Y, Brechet Y, Embury JD (2010) Critical grain size for dislocation storage and consequences for strain hardening of nanocrystalline materials. *Scripta Mater* 63:477–479
- [18] Cizek J, Janecek M, Srba O, Kuzel R, Barnovska Z, Prochazka I, Dobatkin S (2011) Revolution of defects in copper deformed by high-pressure torsion. *Acta Mater* 59:2322–2329
- [19] Shakhova I, Yanushkevich Z, Fedorova I, Belyakov A, Kaibyshev R (2014) Grain refinement in a Cu–Cr–Zr alloy during multidirectional forging. *Mater Sci Eng A* 606:380–389
- [20] Takata N, Ohtake Y, Kita K, Kitagawa K, Tsuji N (2009) Increasing the ductility of ultrafine-grained copper alloy by introducing fine precipitates. *Scripta Mater* 60:590–593
- [21] Meng A, Nie JF, Wei K (2019) Optimization of strength, ductility and electrical conductivity of a Cu–Cr–Zr alloy by cold rolling and annealing treatment. *Vacuum* 167:329–335
- [22] Krishna SC, Karthick NK, Rao GS (2018) High strength utilizable ductility and electrical conductivity in cold rolled sheets of Cu–Cr–Zr–Ti alloy. *J Mater Eng Perform* 27:787–793
- [23] Fu HD, Xu S, Li W (2017) Effect of rolling and annealing processes on microstructure and properties of Cu–Cr–Zr alloy[J]. *Mater Sci Eng A* 700:107–115

- [24] Liang NN, Liu JZ, Lin SC (2018) A multiscale architected Cu-Cr-Zr alloy with high strength, electrical conductivity and thermal stability. *J Alloys Comps* 735:1389–1394
- [25] León KV, Muñoz-Morris MA, Morris DG (2012) Optimisation of strength and ductility of Cu–Cr–Zr by combining severe plastic deformation and precipitation. *Mater Sci Eng A* 536:181–189
- [26] Kermajani M, Raygan S, Hanayi K, Ghaffari H (2013) Influence of thermomechanical treatment on microstructure and properties of electroslag remelted Cu–Cr–Zr alloy. *Mater Des* 51:688–694
- [27] Militzer M, Sun WP, Jonas JJ (1994) Modelling the effect of deformation-induced vacancies on segregation and precipitation. *Acta Metall* 42:133–141
- [28] Guo F, Zhang DF, Yang XS, Jiang LY, Pan FS (2015) Strain-induced dynamic precipitation of Mg₁₇Al₁₂ phases in Mg–8Al alloys sheets rolled at 748K. *Mater Sci Eng A* 636:516–521
- [29] Zhao S, Meng C, Mao F, Hu W, Gottstein G (2014) Influence of severe plastic deformation on dynamic strain aging of ultrafine grained Al–Mg alloys. *Acta Mater* 76:54–67
- [30] Chen XM, Lin YC, Wen DX, Zhang JL, He M (2014) Dynamic recrystallization behavior of a typical nickel-based superalloy during hot deformation. *Mater Des* 57:568–577
- [31] Wang J, Guo W, Gao X, Su J (2015) The third-type of strain aging and the constitutive modeling of a Q235B steel over a wide range of temperatures and strain rates. *Int J Plast* 65:85–107
- [32] Morozova A, Kaibyshev R (2017) Grain refinement and strengthening of a Cu–0.1Cr–0.06Zr alloy subjected to equal channel angular pressing. *Philos Mag* 97:2053–2076
- [33] Mishnev R, Shakhova I, Belyakov A, Kaibyshev R (2015) Deformation microstructures, strengthening mechanisms, and electrical conductivity in a Cu–Cr–Zr alloy. *Mater Sci Eng A* 629:29–40
- [34] Chbihi A, Sauvage X, Blavette D (2012) Atomic scale investigation of Cr precipitation in copper[J]. *Acta Mater* 60:4575–4585
- [35] Chen X, Jiang F, Liu L (2018) Structure and orientation relationship of new precipitates in a Cu–Cr–Zr alloy[J]. *Mater Sci Technol* 34:282–288
- [36] Weast RC (1981) *Handbook of chemistry and physics*, 61st edn. CRC Press, Boca Raton

Publisher's Note Springer Nature remains neutral with regard to jurisdictional claims in published maps and institutional affiliations.